Journal of Materials Chemistry

Cite this: J. Mater. Chem., 2012, 22, 4418

www.rsc.org/materials

PAPER

Full electronic structure across a polymer heterojunction solar cell†

Johannes Frisch,[a] Marcel Schubert,[b] Eduard Preis,[c] Jürgen P. Rabe,[a] Dieter Neher,[b] Ullrich Scherf[c] and Norbert Koch*[a]

Received 3rd October 2011, Accepted 15th November 2011
DOI: 10.1039/c1jm14968g

We correlate the morphology and energy level alignment of bilayer structures comprising the donor poly(3-hexylthiophene) (P3HT) and the acceptor polyfluorene copolymer poly(9,9′dialklylfluorene-*alt*-4,7-bis(2,5-thiendiyl)-2,1,3-benzothiadiazole) (PFTBTT) with the performance of these bilayers in organic photovoltaic cells (OPVCs). The conducting polymer poly(ethylenedioxythiophene):poly (styrenesulfonate) (PEDT:PSS) was used as the bottom electrode and Ca as the top electrode. Ultraviolet photoelectron spectroscopy (UPS) revealed that notable interface dipoles occur at all interfaces across the OPVC structure, highlighting that vacuum level alignment cannot reliably be used to estimate the electronic properties for device design. Particularly the effective electrode work function values (after contact formation with the conjugated polymers) differ significantly from those of the pristine electrode materials. Chemical reactions between PEDT:PSS and P3HT on the one hand and Ca and PFTBTT on the other hand are identified as cause for the measured interface dipoles. The vacuum level shift between P3HT and PFTBTT is related to mutual energy level pinning at gap states. Annealing induced morphological changes at the P3HT/PFTBTT interface increased the efficiency of OPVCs, while the electronic structure was not affected by thermal treatment.

Introduction

The power conversion efficiency of organic polymer-based photovoltaic cells (OPVCs) improved significantly in the past two years, now exceeding 8%.[1] The barrier of 10% (power conversion efficiency for amorphous silicon) has to be overcome to establish OPVCs as a reliable future technology. Some of the most efficient polymer-based solar cells are still limited by a low open circuit voltage (V_{OC}), which is largely determined by the high electron affinity of the fullerene-based acceptor units. All-polymer heterojunction OPVCs are highly suited to optimizing the photovoltaic gap [energy difference between the valence band (VB) maximum of the donor and the conduction band (CB) minimum of the acceptor] because the conjugated polymer VB and CB energies as well as the band gap can be finely tuned via synthesis.[2,3] However, while the number of new high-potential polymers for good photovoltaic performance is steadily increasing, investigations of the energy level alignment at polymer/polymer interfaces are rare. Even though significant vacuum level shifts across a heterojunction (as already reported for small molecule-based heterojunctions[4]) can strongly influence the actual photovoltaic gap of a donor/acceptor pair, vacuum level alignment at polymer/polymer heterojunctions is commonly assumed. One reason for the lack of such investigation is the difficulty in preparing well-defined polymer heterojunctions excluding intermixing of the two materials.

In the present study we investigate the energy level alignment across all interfaces that occur in a polymer-heterojunction OPVC comprising poly(3-hexylthiophene) (P3HT) as donor and poly (9,9′difarnesylfluorene-*alt*-4,7-bis(2,5-thiendiyl)-2,1,3-benzothiadiazole) (PFTBTT) as acceptor (chemical structures and OPVC structure shown in Fig. 1). This particular material combination allows reaching high open circuit voltage (V_{OC}) values.[5] Furthermore, using an interlayer approach we minimize intermixing of both materials at their interface.[6,7] We focus on the evolution of the energy levels and morphology during sequential deposition of the active materials on the bottom electrode and upon forming the top electrode by measuring work function, valence and core levels using photoemission spectroscopy. We find that significant vacuum level shifts occur at interfaces between the electrodes and the polymers, as well as at the polymer heterojunction. These results emphasize that simple models, such as vacuum level alignment, to estimate the energy levels in an OPVC fail, and that more experimental and theoretical work is required to derive reliable energy level alignment rules in the future.

[a]Institut für Physik, Humboldt-Universität zu Berlin, Newtonstr. 15, 12489 Berlin, Germany. E-mail: norbert.koch@physik.hu-berlin.de; Fax: +49 30 2093 7632; Tel: +49 30 2093 7819
[b]Institut für Physik und Astronomie, Universität Potsdam, Karl-Liebknecht-Str.24/25, 14476 Potsdam, Germany. E-mail: Neher@uni-potsdam.de; Fax: +49 331 977 5615; Tel: +49 331 977 1751
[c]Fachbereich C—Makromolekulare Chemie, Bergische Universität Wuppertal, Gaußstr. 20, 42119 Wuppertal, Germany. E-mail: scherf@uni-wuppertal.de; Fax: +49 202 439 3880; Tel: +49 202 439 2493
† Electronic supplementary information (ESI) available. See DOI: 10.1039/c1jm14968g

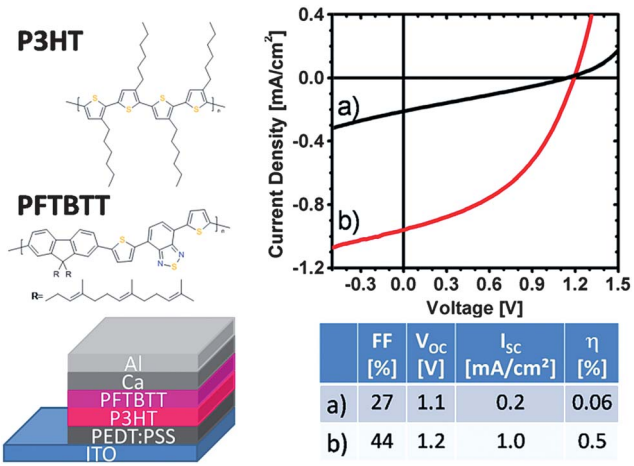

	FF [%]	V_{OC} [V]	I_{SC} [mA/cm²]	η [%]
a)	27	1.1	0.2	0.06
b)	44	1.2	1.0	0.5

Fig. 1 The left side shows the chemical structure of poly(3-hexylthiophene) (P3HT) and poly(9,9'difarnesylfluorene-*alt*-4,7-bis(2,5-thiendiyl)-2,1,3-benzothiadiazole) (PFTBTT) along with the photovoltaic cell structure. The inset table reports fill factor (FF), open circuit voltage (V_{OC}) and power conversion efficiency (η) of (a) as-prepared and (b) pre-annealed OPVCs with PFTBTT* as acceptor polymer.

Experimental section

Materials

P3HT was synthesized in high purity and with mean average molecular weights >40 000 g mol^{-1} with a polydispersity of 1.3 in a GRIM-methathese protocol according to the literature.[8]

The alternating copolymer poly(9,9′difarnesylfluorene-*alt*-4,7-bis(2,5-thiendiyl)-2,1,3-benzothiadiazole) (PFTBTT) was generated in a Suzuki-type cross-coupling reaction using the diboronic ester of the fluorene compound and the dibrominated TBTT as monomers.[9] The resulting copolymer exhibits a molecular weight of *ca.* 5000 g mol^{-1} (M_n) with a polydispersity around 2. A Stille-type cross-coupling of distannylated bisthienylbenzothiadiazole (TBTT) with dibromofluorene resulted in copolymers with similar molecular weights. In order to check the influence of the length of the side chains on the molecular weight (M_n), we switched from the 2-ethylhexyl- to 2,6,10-trimethyl dodecyl side chains (see Table 1).

For OPVC fabrication a slightly shorter octyl side group in the acceptor polymer (PFTBTT*) was used. The molecular weight of the modified PFTBTT* was M_w(PFTBTT*) = 12 400 g mol^{-1}. We stress that UPS measurements showed no difference in the ionization energy and energy level alignment as a function of different side chains.

Table 1 Properties of the acceptor polymer depending on the type of polymerization[a]

Type of polymerisation	Side chains	λ_{max}/nm	(M_n/M_w)/ g mol^{-1}	% TBTT (EA)	% TBTT (UV)
alt/Suzuki/Fbo	EtHex	385.5	4000/6000	47.4	47.5
alt/Stille/Fbr	EtHex	383.5	5000/10 000	47.2	47.6
alt/Stille/Fbr	Trimethyl dodecyl	384.5	5000/10 000	51.7	51.7

[a] EA: Elemental analysis; UV: UV/Vis-spectroscopy.

Photoemission spectroscopy

Ultraviolet and X-ray photoelectron spectroscopy (UPS and XPS) measurements were conducted at Humboldt-Universität using He I radiation ($h\nu$ = 21.22 eV) of a helium discharge lamp and Mg Kα radiation ($h\nu$ = 1253.6 eV) of a non-monochromatized X-ray source. Photo-excited electrons were detected with a Specs Phoibos 100 hemispherical energy analyzer. The error of energy values reported below is estimated to be 0.05 eV for UPS and 0.1 eV for XPS. The secondary electron cutoff (SECO) spectra were obtained with the samples biased at −10 V in order to clear the analyzer work function. Sample preparation and device fabrication conditions were essentially identical. A commercially available conducting polymer blend poly(ethylenedioxythiophene):poly(styrenesulfonate) (PEDT:PSS) (Baytron® P AI4083 H. C. Stark-Heraeus) was spin coated (1500 rpm) on UV/O_3 treated (30 min) indium-tin oxide glass substrates (sheet resistance 15–30 Ω) from aqueous dispersion and dried at 200 °C for 5 min under ambient conditions. Donor and acceptor polymer film deposition was done in a N_2-filled glovebox (concentration of O_2 and H_2O <1 ppm). P3HT was spin coated from chloroform solution (6 mg ml^{-1}, 1500 rpm) and annealed *in situ* at 180 °C for 30 min. Films were subsequently washed with chloroform to render an insolubilized P3HT-interlayer (P3HT-IL) (~3 nm). PFTBTT was spin coated from chloroform solution (1 mg ml^{-1}, 3000 rpm) on top of the P3HT-IL. PFTBTT films were annealed at 140 °C for 10 min in the glovebox. When noted, film thicknesses were obtained by determining the absorption of thin films, while the absorption coefficients were calculated beforehand from the absorption spectra of thicker films, whose thickness was measured by a surface profilometer. Calcium was vacuum sublimed (base pressure < 3 × 10^{-9} mbar) from a resistively heated crucible source (at a rate of 0.05 Å s^{-1}) in the preparation chamber. Transfer from preparation to analysis chamber was realized without breaking vacuum. The metal film mass-thickness was monitored with a quartz crystal microbalance (QCM), therefore every layer thickness provided in this work corresponds to a nominal mass-thickness as read from the QCM.

In some cases, samples were illuminated during photoemission measurements with a halogen lamp (SoLux, 4700K, 35 W, 36°) from EIKO that provides a replication of daylight with an illuminance of 1864 Lux at a distance of 0.4 m (lamp-to-sample distance in our experiments).

XPS spectra were fitted using the software WINSPEC (developed at the University of Namur, Belgium). Binding energies are reported relative to the Fermi-energy for UPS spectra. For all XPS spectra the Shirley background correction was used.[10]

Fabrication and characterization of OPVCs

OPVCs were prepared following essentially the same routine as described for the UPS/XPS samples. All devices were prepared on poly(ethylenedioxythiophene):poly(styrenesulfonate) (PEDT:PSS)-coated ITO substrates with a thin (3 nm) P3HT-interlayer (P3HT-IL) on top and a 40 nm thick PFTBTT layer (spin coated from chloroform with a concentration of 6 mg ml^{-1} and 1500 rpm) covered by 20 nm Ca and 75 nm Al as the top

electrode. Current–voltage characteristics were recorded with a Keithley 2400 Digital SourceMeter under AM 1.5G illumination from a KHS Steuernagel solar simulator, working at an irradiance of 100 mW cm^{-2}. Pre-annealed devices were annealed at 140 °C for 10 min before the top Ca/Al electrode was deposited.

Scanning force microscopy

SFM measurements were performed in tapping mode and ambient conditions using a JPK NanoWizard. The same samples as used for the photoemission experiments were used to analyze the surface morphology.

Results and discussion

Photovoltaic performance

Fig. 1 shows that the performance of P3HT/PFTBTT bi-layer devices is substantially enhanced by pre-annealing, *i.e.*, before application of the Ca/Al electrode. The pre-annealed devices yielded power conversion efficiencies of 0.5% compared to only 0.06% for as-spun devices. This improvement is brought about through an increase in short circuit current (J_{SC}) (from 0.2 to 1.0 mA cm^{-2}), open-circuit voltage (from 1.1 to 1.2 V), and fill factor (from 27 to 44%). We note that device parameters obtained here are lower than those reported for a similar material combination.[11] However, devices studied here were inherently limited by the small interfacial area due to the strict bi-layer geometry and they were not further optimized with respect to layer thickness or annealing parameters. The aim of this work, conversely, was not to achieve highest possible efficiencies but rather to understand the fundamental electronic properties that give rise to device function.

P3HT/PFTBTT interface

To assess the energy level alignment across interfaces in the device, UPS measurements were performed for the PEDT:PSS substrate first, then for the P3HT-IL, and finally for PFTBTT deposited on the P3HT-IL. (Results for the top-electrode deposition are reported separately further below.) Valence region and corresponding SECO spectra are shown in Fig. 2. The pristine PEDT:PSS work function (ϕ) of 5.0 eV is decreased to 4.2 eV upon deposition of the P3HT-IL (Fig. 2(a) and (b)). Because the ionization energy (IE) of P3HT (IE = 4.5 eV) is much lower than ϕ of PEDT:PSS (5.0 eV) the valence band onset of P3HT is pinned 0.3 eV below the Fermi-level (E_F) due to interfacial charge transfer. This leads to a formation of an interface dipole of 0.8 eV as described earlier.[12] The interface dipole contributes greatly to the effective ϕ of the anode. It is thus important to note that the effective ϕ is the relevant value and not that of bare PEDT:PSS when correlating material parameters and device performance.

The VB spectra of PFTBTT spin coated on the P3HT-IL (Fig. 2(c)) show no more intensity close to E_F originating from the underlying P3HT-IL. Because of the short mean free path of the emitted photoelectrons in UPS measurements (0.4 nm at an electron kinetic energy ~20 eV[13]), the absence of P3HT features is evidence for a complete coverage of the P3HT-IL by the

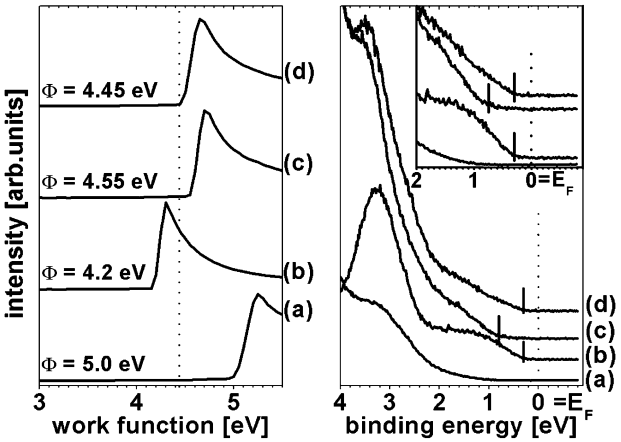

Fig. 2 Photoemission spectra of the valence region (right side) and secondary electron cutoff (left side) of (a) pristine PEDT:PSS, (b) P3HT-IL, (c) PFTBTT spin coated on top of P3HT-IL as-prepared and (d) after annealing for 10 min at 140 °C. The inset shows a zoom of the valence band near the Fermi-energy. Vertical lines indicate the valence band onset.

PFTBTT film and the absence of pronounced polymer intermixing. The PFTBTT film thickness was estimated to be ~7 nm. The sample ϕ (see SECO in Fig. 2(c)) increases to 4.55 eV upon deposition of PFTBTT and the VB onset is located at 0.8 eV binding energy (BE). The resulting ionization energy of 5.35 eV is comparable to that measured for PFTBTT films spin coated directly on PEDT:PSS (see ESI†) and to literature values.[14] The shift of ϕ due to the deposition of PFTBTT is unexpected considering the high IE of PFTBTT compared to the effective ϕ (of the PEDT:PSS/P3HT-IL substrate). For such a situation vacuum level alignment might be expected.[15] However, gap states of extremely low density may exist in PFTBTT, which do not show up in photoemission but can cause pinning of E_F.[16]

UPS results for the PEDT:PSS/P3HT-IL/PFTBTT interfaces without top electrode are summarized in the energy level diagram in Fig. 3. The position of the P3HT conduction band (CB) onset was calculated by subtracting the transport gap of 2.4 eV from the VB onset position.[17] The transport gap of PFTBTT was estimated to be 2.4 eV, with the optical gap of 1.9 eV (determined by measuring the absorption onset of a thin film) and assuming the same exciton binding energy (0.5 eV) as for P3HT.[17]

It is accepted that V_{OC} is limited by the photovoltaic gap (difference between the valence band onset of the donor and the conduction band onset of the acceptor).[18,19] For the materials used here a maximum V_{OC} of 1.9 eV would be deduced from the energy level diagram in Fig. 3. This value is larger than the energy difference between the ionization energy of P3HT (4.5 eV) and the electron affinity of PFTBTT (2.95 eV) assuming vacuum level alignment, which yields 1.55 eV. This underlines the importance of UPS measurements to assess the actual energy level alignment at heterojunctions, which is vital for evaluating new material combinations. More strikingly, the UPS-derived value is much larger than the measured V_{OC} of 1.2 eV in the device (see Fig. 1). Consequently, another V_{oc}-limiting mechanism must be operative (*vide infra*).

Fig. 2(d) shows SECO and VB spectra of an annealed PFTBTT film on top of the P3HT-IL. Annealing results in

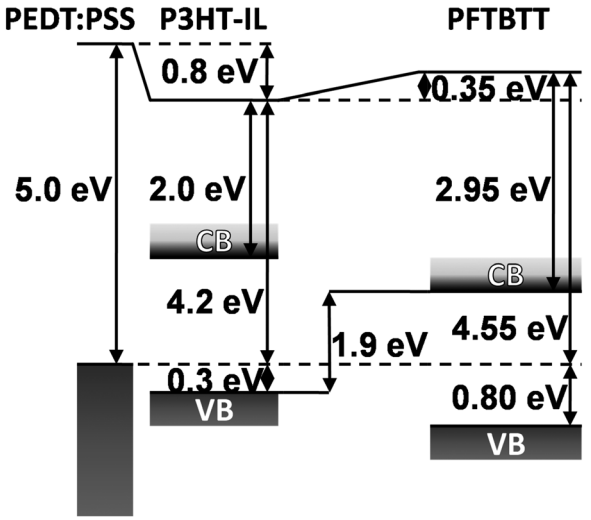

Fig. 3 Schematic energy level diagram of the P3HT-IL/PFTBTT heterojunction. The position of the conduction band onset was calculated using the transport gap for P3HT and PFTBTT. The latter was estimated by adding the same exciton binding energy as for P3HT to the optical gap of PFTBTT (determined by UV-vis absorption measurements).

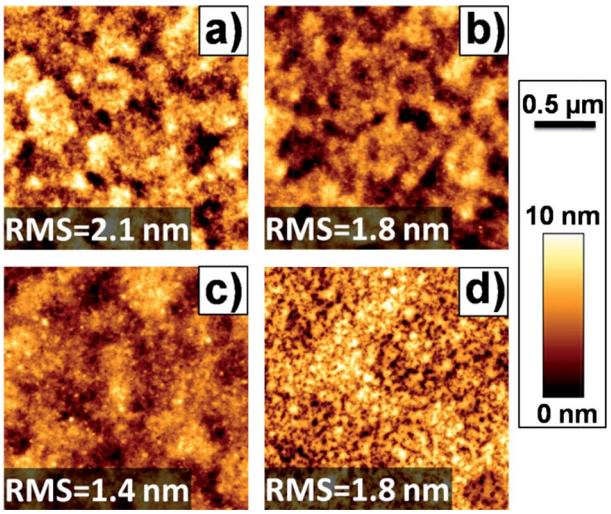

Fig. 4 SFM height images of (a) PEDT:PSS, (b) P3HT-IL, (c) PFTBTT spin coated on top of P3HT-IL as-prepared and (d) after annealing for 10 min at 140 °C.

a different shape and onset of the VB spectra in comparison to the as-prepared PFTBTT film. As for the bare P3HT-IL the VB onset is at 0.3 eV BE. Since annealed PFTBTT films spin coated directly on PEDT:PSS exhibit the same VB onset as not-annealed ones, the new VB onset can be explained by the emergence of bare P3HT patches at the sample surface and/or intermixing of PFTBTT and P3HT. This assumption is supported by a small ϕ decrease of 0.1 eV due to annealing. Because ϕ measured by UPS is an area-averaged value, small patches of bare P3HT at the surface with the lower local ϕ of 4.2 eV can reasonably explain the experimental findings. It is important to note that for thicker PFTBTT films (~25 nm) the VB onset position after annealing is constant (see ESI†). This indicates that annealing only affects the morphology directly at the P3HT/PFTBTT interface.

The influence of annealing on film morphology as suggested above is further evidenced by scanning force microscopy (SFM) measurements (Fig. 4). The root-mean-square (RMS) roughness of PEDT:PSS (RMS 2.1 nm) decreases upon deposition of the P3HT-IL (RMS 1.8 nm) and PFTBTT (RMS 1.4 nm). However, the roughness of the annealed sample is increased (RMS 1.8 nm). As can be directly seen by comparing Fig. 4(c) and (d) distinct features on the few 10 nm scale develop at the surface of PFTBTT upon annealing.

Combining the UPS and SFM results, we can conclude that annealing induces an interpenetration of both materials and simultaneously a phase separation. This behavior was already suggested before for blend films.[20–22] Both effects increase the exciton dissociation efficiency because of a larger interfacial area. In OPVCs this effect results in an increase of J_{SC} from 0.2 mA cm^{-2} for as-prepared devices to 1 mA cm^{-2} for pre-annealed devices (*vide supra*).

PFTBTT/Ca interface

XPS spectra recorded for different Ca mass-thickness deposited on an annealed PEDT:PSS/P3HT-IL/PFTBTT sample are shown in Fig. 5. Upon Ca deposition a new peak develops in the S2p core level spectra at lower BE indicating a strong chemical interaction between S atoms in the polymer and Ca. For the first three deposition steps the new peak's intensity increases whereas the two S component intensities at higher BE decrease. The two high BE components are attributed to the thiophene and benzothiadiazole units, respectively (see Fig. 5).

The Ca2p core levels initially start with one high BE component, with a low BE component developing and even dominating for higher Ca coverage. Interestingly, up to a nominal mass-thickness of 8 Å Ca the total peak area of the S2p spectrum does not decrease (for fitted peak area and peak positions see Table 2). In this regime only the high BE component of the Ca2p spectrum exists, indicating that this component represents the Ca atoms reacted with S. Nevertheless, as soon as the low BE component in

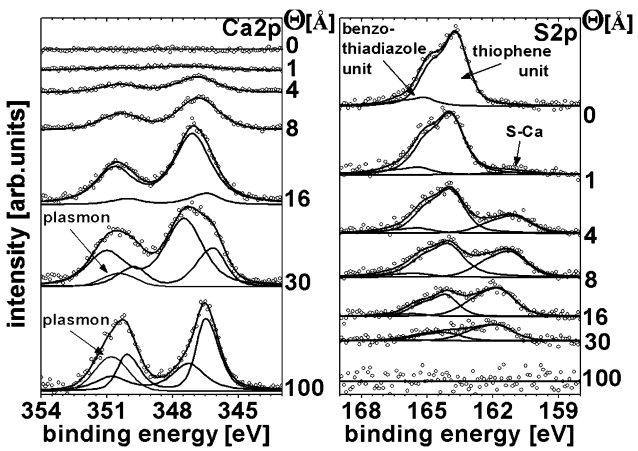

Fig. 5 XPS spectra of Ca2p (left side) and S2p (right side) core levels for increasing calcium coverage (Θ) on the annealed P3HT-IL/PFTBTT heterojunction (PFTBTT film thickness ~7 nm). Dots represent the original data whereas lines are the results of the fitting routine. The grey peaks in the Ca2p spectrum represent photo emitted electrons that were scattered at bulk-plasmons.

the Ca2p spectrum appears, the features in the S2p spectrum also start to attenuate. This rather slow decrease of the S2p intensity suggests that in the beginning of the metal deposition Ca atoms rather penetrate into the polymer film and a closed metal film entirely covering the surface develops only for coverage greater than 30 Å. Similar observations were reported for the deposition of Ca on P3HT, where the interface formation is initially dominated by the formation of Ca–S clusters in the polymer film followed by the formation of large 3D Ca clusters on the polymer surface.[23,24]

Fig. 6 shows SECO and VB spectra for different Ca thicknesses. ϕ drastically decreases to 2.8 eV for 16 Å Ca coverage. For 30 Å Ca coverage and beyond ϕ stabilizes at 3.0 eV. As already observed in XPS, the overall intensity of polymer-related VB features decreases only slowly. However, quantification of the VB onset shifts and those of the localized π-band (marked by arrows in VB spectra of Fig. 6) due to Ca deposition is difficult because of significant broadening. The localized π-band (maximum initially at ~3.4 eV) feature is only distinguishable up to a Ca coverage of 4 Å. Nevertheless, it can be seen in Fig. 6 that this feature shifts to higher BE. No well-defined gap states are generated. This behavior is typical for the formation of Ca/conjugated polymer interfaces involving Ca–polymer reactions, particularly when the polymer contains thiophene units.[25–27] Thermodynamic equilibrium is established across the entire sample as concluded from the correct position of emission from the Ca Fermi-edge (see Fig. 6). If we assume vacuum level alignment at the PFTBTT/Ca interface, all energy levels of the PFTBTT should shift to higher BE by the same amount as ϕ changes due to E_F alignment, *i.e.*, we expect the polymer energy level shift to represent the magnitude of the built-in field between the two electrodes. A shift to higher BE of the VB features was already noted before but the spectral broadening inhibited the quantitative analysis. Instead, we evaluated the components in the S2p core level spectra more closely. Fig. 7 summarizes the evolution of the peak shifts of the S2p levels (specifically those of unreacted thiophene units and those of S reacted with Ca), as well as the ϕ changes as a function of nominal Ca coverage. For increasing Ca thickness ϕ decreases and the BE of sulfur components increases, but in contrast to a situation of vacuum level alignment at the PFTBTT/Ca interface, the magnitude of the shifts largely differs. While in total ϕ decreases by 1.55 eV, the

Table 2 Area and position of the components in the S2p core level spectra corresponding to the sulfur in the thiophene unit and the sulfur reacted with Ca. The fitted spectra are shown in Fig. 5. The values for the area and position are obtained by a fitting routine. In the last column the total area of both components is presented

Nominal mass-thickness of Ca/Å	Sulfur–thiophene unit		Sulfur reacted with Ca		Sum
	Area [arb. u.]	Position/ eV	Area [arb. u.]	Position/ eV	Area [arb. u.]
0	322	163.7	—	—	322
1	292	163.8	39	160.7	331
4	243	163.9	102	161.0	345
8	230	164.0	137	161.1	367
16	115	164.2	159	161.7	274
30	60	164.2	83	161.7	143

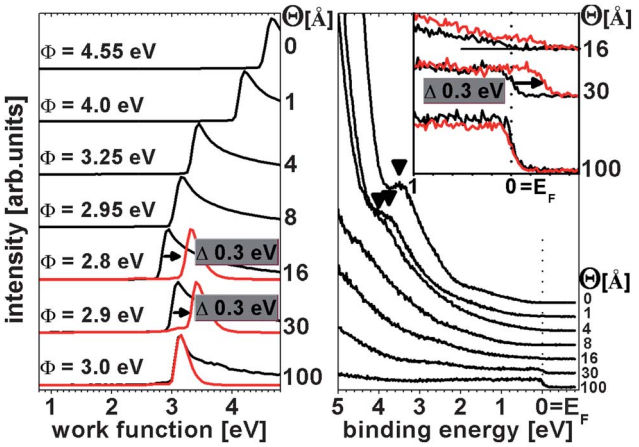

Fig. 6 UPS spectra of the valence region (right side) and secondary electron cutoff (left side) for increasing calcium coverage (Θ) on the annealed P3HT-IL/PFTBTT heterojunction. Black spectra were taken in the dark, spectra in red are from samples that were illuminated with white light during the measurement. Black triangles indicate the position of the lowest localized π-band of PFTBTT.

BE of the thiophene–sulfur component only increases by 0.5 eV. The resulting difference of 1.05 eV is thus attributed to an interface dipole. Dipole formation at the PFTBTT/Ca interface is plausible because the Ca–S bond formation involves net electron transfer to the polymer. Furthermore, the reaction likely creates gap states close to the polymer CB, where E_F of metallic Ca is pinned. The resulting energy level diagram across the entire PEDT:PSS/P3HT-IL/PFTBTT/Ca system (Fig. 8) shows that the vacuum level alignment model fails completely to predict the actual situation in the OPVC. The ϕ difference of the bare PEDT:PSS and Ca electrodes (2 eV), as predicted by the metal–insulator–metal model,[28] is not consistent with the *effective* electrode ϕ difference. The relevant values thus are 4.2 eV for the PEDT:PSS/P3HT-IL system and 2.8–3.0 eV for the PFTBTT/Ca system. Noteworthy, the effective ϕ difference in the OPVC amounts to 1.2–1.4 eV, which is remarkably close to the V_{oc}

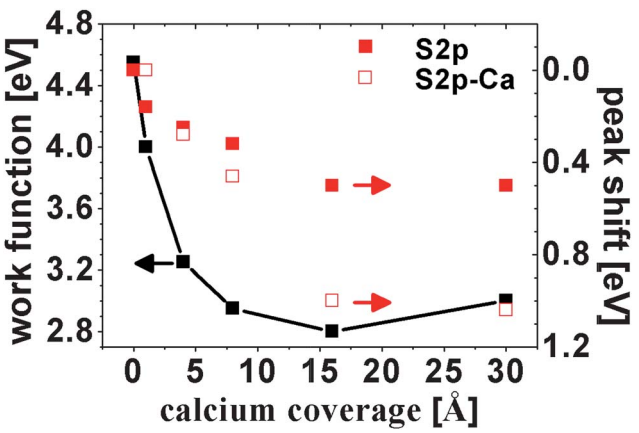

Fig. 7 Work function and peak shifts of the S2p core levels for increasing calcium coverage. Peak shifts are taken from fits shown in Fig. 6. Solid squares represent the shift of the major component in the higher binding energy peak and open squares represent the shift of the new component at lower binding energy.

obtained for the devices (see Fig. 1). Consequently, our study suggests that in the present OPVC architecture with a very thin (~3 nm) donor layer two limiting mechanisms for V_{oc} exist: (i) the photovoltaic gap and (ii) the effective ϕ difference of the electrodes. The lower of the two limits sets the V_{oc} limit.

Light induced surface voltage

By additionally illuminating the sample with light in the visible and near-infrared spectral range during UPS experiments equilibrium between the two electrodes can no longer be sustained. As shown in Fig. 6 for 16 Å and 30 Å Ca coverage, both valence band and SECO (red curves) shift rigidly by ~0.3 eV to lower BE due to illumination. The Ca derived states close to and at E_F clearly appear above E_F of the substrate electrode. Consequently, without illumination the electrostatic potential distribution across the layer stack is comparable to short circuit conditions in the device (described above for measurements in the dark); the situation during illumination is comparable to open circuit conditions because the bottom and the top electrodes are not connected. Obviously, exciton dissociation occurs at the P3HT/PFTBTT interface (as it does in working OPVCs) and negative charges are collected at the Ca side and holes flow to the bottom electrode, thus building up negative space charge at the very surface of the sample. This can occur as long as the top Ca layer has no direct contact to the grounded sample holder. As soon as the Ca coverage is sufficient to form a continuous film that allows making direct electrical contact to the grounded sample holder, equilibrium between the electrodes is re-established and no more light-induced shifts of the top E_F position occur (spectra for 100 Å Ca coverage in Fig. 6).

The shift of E_F corresponds to the electrostatic potential difference between the PEDT:PSS anode and the Ca cathode that is reached when the net current between electrodes becomes zero. Because of the interpenetrating network formed at the annealed P3HT-IL/PFTBTT interface and the small overall PFTBTT thickness Ca may partially be in direct contact to the P3HT-IL. This shunt resistor in parallel with the active part of the "device" and the photocurrent that leaves the sample surface (during the UPS measurement) may be responsible for the fact that the light-induced shift of 0.3 V is much lower than the V_{OC} (1.2 eV) of actual OPVCs. Furthermore, since the open circuit voltage depends on the illumination intensity[29] the rather low intensity of the halogen lamp employed to illuminate the sample in the UPS chamber also contributes to the comparably small shift. However, with an appropriately adapted experimental setup UPS may be used to measure V_{oc} in addition to the electronic properties of OPVC structures in equilibrium. Conversely, great care must be taken when performing photoemission experiments with samples resembling an OPVC since light-induced non-equilibrium conditions may persist.

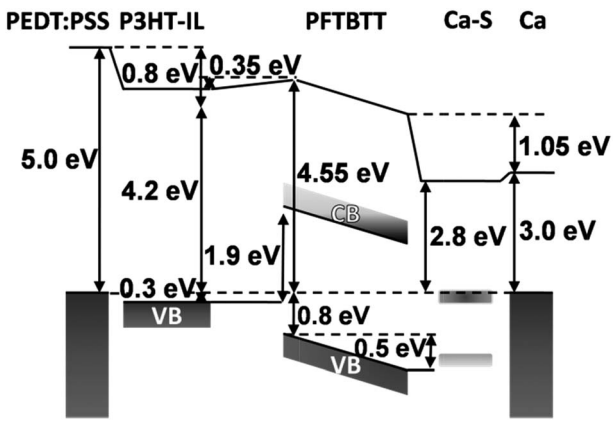

Fig. 8 Schematic energy level diagram at the PFTBTT/calcium interface on top of a P3HT-IL/PFTBTT heterojunction.

Conclusion

We presented a comprehensive study of the energy level alignment across a functional OPVC structure consisting of a PEDT:PSS bottom electrode, a P3HT/PFTBTT donor/acceptor bilayer, and Ca as the top electrode, and we correlated the results with OPVC performance. Annealing of the polymer layers prior to Ca electrode deposition increased the OPVC power conversion efficiency by nearly one order of magnitude. UPS and SFM showed that annealing induces an interpenetrating phase-separated network of P3HT/PFTBTT, which increases the active area but leaves the electronic level unaffected. Regarding the interfacial electronic structure, we found that, in contrast to the often assumed vacuum level alignment at polymer/polymer heterojunctions, a vacuum level shift of −0.35 eV at the P3HT/PFTBTT interface occurred. The PFTBTT/Ca interface formation was accompanied by a strong chemical reaction between Ca and S in the polymer, which in addition to the appearance of gap states led to an interfacial vacuum level shift of *ca.* 1 eV. Illumination of OPVC-like sample structures with visible light during UPS measurements induced a non-equilibrium situation, as evidenced by a Fermi-level shift between bottom and top electrodes. UPS may thus, in principle, be used to derive V_{OC} values for OPVCs in addition to the full information of the electronic structure.

Acknowledgements

This work was supported by the SPP1355 of the DFG. We thank Georg Heimel for valuable discussions and Andreas Elschner (H. C. Starck-Heraeus) for providing PEDT:PSS.

Notes and references

1 M. A. Green, K. Emery, Y. Hishikawa, W. Warta and E. D. Dunlop, *Prog. Photovoltaics*, 2011, **19**, 565–572.
2 K. Vandewal, K. Tvingstedt, A. Gadisa, O. Inganas and J. V. K. Manca, *Nat. Mater.*, 2009, **8**, 904–909.
3 M. Scharber, D. Mühlbacher, M. Koppe, P. Denk, C. Waldauf, A. Heeger and C. Brabec, *Adv. Mater.*, 2006, **18**, 789–794.
4 H. Vazquez, F. Flores and A. Kahn, *Org. Electron.*, 2007, **8**, 241–248.
5 D. Mori, H. Benten, J. Kosaka, H. Ohkita, S. Ito and K. Miyake, *ACS Appl. Mater. Interfaces*, 2011, **3**, 2924–2927.
6 J.-S. Kim, R. H. Friend, I. Grizzi and J. H. Burroughes, *Appl. Phys. Lett.*, 2005, **87**, 023506.
7 C. Yin, B. Pieper, B. Stiller, T. Kietzke and D. Neher, *Appl. Phys. Lett.*, 2007, **90**, 133502.
8 R. S. Loewe, S. M. Khersonsky and R. D. McCullough, *Adv. Mater.*, 1999, **11**(3), 250.
9 M. Svensson, F. Zhang, S. C. Veenstra, W. J. H. Verhees, J. C. Hummelen, J. M. Kroon, O. Inganäs and M. R. Anderson, *Adv. Mater.*, 2003, **15**(12), 988.

10 S. Tougaard and P. Sigmund, *Phys. Rev. B*, 1982, **25**, 4452–4466.
11 C. R. McNeill, A. Abrusci, J. Zaumseil, R. Wilson, M. J. McKiernan, J. H. Burroughes, J. J. M. Halls, N. C. Greenham and R. H. Friend, *Appl. Phys. Lett.*, 2007, **90**, 193506.
12 J. Frisch, A. Vollmer, J. P. Rabe and N. Koch, *Org. Electron.*, 2011, **12**, 916–922.
13 M. P. Seah and W. D. Dench, *Surf. Interface Anal.*, 1979, **1**(1), 2.
14 C. R. McNeill, J. J. M. Halls, R. Wilson, G. L. Whiting, S. Berkebile, M. G. Ramsey, R. H. Friend and N. C. Greenham, *Adv. Funct. Mater.*, 2008, **18**, 2309–2321.
15 S. Braun, W. R. Salaneck and M. Fahlmann, *Adv. Mater.*, 2009, **21**, 1450–1472.
16 I. Lange, J. C. Blakesley, J. Frisch, A. Vollmer, N. Koch and D. Neher, *Phys. Rev. Lett.*, 2011, **106**, 216402.
17 K. Kanai, T. Miyazaki, H. Suzuki, M. Inaba, Y. Ouchi and K. Seki, *Phys. Chem. Chem. Phys.*, 2010, **12**, 273–282.
18 G. Dennler, M. C. Scharber and C. J. Brabec, *Adv. Mater.*, 2009, **21**, 1323–1338.
19 B. P. Rand, D. P. Burk and S. R. Forrest, *Phys. Rev. B: Condens. Matter Mater. Phys.*, 2007, **75**, 115327.
20 C. R. MCNeill, B. Watts, S. Swaraj, H. Ade, L. Thomsen, W. Belcher and P. C. Dastoor, *Nanotechnology*, 2008, **19**, 424015.
21 C. R. McNeill, A. Abrusci, I. Hwang, M. A. Ruderer, P. Müller-Buschbaum and N. C. Greenham, *Adv. Funct. Mater.*, 2009, **19**, 3103–3111.
22 R. C. Mulherin, S. Jung, K. Johnson, P. Kohn, M. Sommer, S. Allard, U. Scherf and N. C. Greenham, *Nano Lett.*, 2011, **11**, 4846.
23 J. Zhu, F. Bebensee, W. Hieringer, W. Zhao, J. H. Baricuatro, J. A. Farmer, Y. Bai, H.-P. Steinrück, J. Michael Gottfried and C. T. Campbell, *J. Am. Chem. Soc.*, 2009, **131**, 13498–13507.
24 F. J. J. Jansen, L. J. van IJzendorn, A. W. Denier van der Gon, M. J. A. de Voigt and H. H. Brongersma, *Phys. Rev. B: Condens. Matter Mater. Phys.*, 2004, **70**, 165425.
25 M. K. Fung, S. L. Lai, S. W. Tong, S. N. Bao, C. S. Lee, W. W. Wu, M. Inbasekaran, J. J. O'Brien and S. T. Lee, *J. Appl. Phys.*, 94, 5764–5770.
26 L. S. Liao, L. F. Chneg, M. K. Fung, C. S. Lee, S. T. Lee, M. Inbasekaran, E. P. Woo and W. W. Wu, *Phys. Rev. B: Condens. Matter Mater. Phys.*, 2000, **62**, 10004–10007.
27 A. Rajagopal, N. Koch, J. Ghijsen, R. L. Johnson, K. Kaeriyama, G. Leisig and J.-J. Pireaux, *J. Appl. Phys.*, 2000, **87**, 1331–1336.
28 P. W. M. Blom, V. D. Mihailetchi, L. J. A. Koster and D. E. Markov, *Adv. Mater.*, 2007, **19**, 1551–1566.
29 L. J. A. Koster, V. D. Mihailetchi, R. Ramaker and P. W. M. Blom, *Appl. Phys. Lett.*, 2005, **86**, 123509.

